RESEARCH ARTICLE | OCTOBER 06 2023

Development of spinning-disk solid sample delivery system for high-repetition rate x-ray free electron laser experiments

N. Welke ; N. Majernik ; R. Ash ; A. Moro; R. Agustsson ; P. Manwani ; K. Li ; A. Sakdinawat; A. Aquila ; A. Benediktovitch; A. Halavanau ; J. Rosenzweig; U. Bergmann ; C. Pellegrini

Rev. Sci. Instrum. 94, 103005 (2023)
https://doi.org/10.1063/5.0168125
CHORUS

Review of Scientific Instruments ARTICLE pubs.aip.org/aip/rsi

Development of spinning-disk solid sample delivery system for high-repetition rate x-ray free electron laser experiments

Cite as: Rev. Sci. Instrum. 94, 103005 (2023); doi: 10.1063/5.0168125
Submitted: 17 July 2023 • Accepted: 12 September 2023 •
Published Online: 6 October 2023

N. Welke,[1] N. Majernik,[2] R. Ash,[1] A. Moro,[3] R. Agustsson,[3] P. Manwani,[2] K. Li,[4] A. Sakdinawat,[4] A. Aquila,[4] A. Benediktovitch,[5] A. Halavanau,[4,a)] J. Rosenzweig,[2] U. Bergmann,[1,a)] and C. Pellegrini[4,a)]

AFFILIATIONS

[1] Department of Physics, University of Wisconsin Madison, Madison, Wisconsin 53706, USA
[2] Department of Physics, University of California Los Angeles, Los Angeles, California 90095, USA
[3] RadiaBeam Technologies, Santa Monica, California 90404, USA
[4] SLAC National Accelerator Laboratory, Menlo Park, California 94025, USA
[5] Center for Free-Electron Laser Science CFEL, Deutsches Elektronen-Synchrotron DESY, Notkestr. 85, 22607 Hamburg, Germany

[a)] **Authors to whom correspondence should be addressed:** aliaksei@slac.stanford.edu, ubergmann@wisc.edu, and claudiop@slac.stanford.edu

ABSTRACT

X-ray free-electron lasers (XFELs) deliver intense x-ray pulses that destroy the sample in a single shot by a Coulomb explosion. Experiments using XFEL pulse trains or the new generation of high-repetition rate XFELs require rapid sample replacement beyond those provided by the systems now used at low repletion-rate XFELs. We describe the development and characterization of a system based on a spinning disk to continuously deliver a solid sample into an XFEL interaction point at very high speeds. We tested our system at the Linac Coherent Light Source and European XFEL hard x-ray nano-focus instruments, employing it to deliver a 25 μm copper foil sample, which can be used as a gain medium for stimulated x-ray emission for the proposed x-ray laser oscillator.

I. INTRODUCTION

X-ray free electron lasers (XFELs) emit x-ray pulses with an extreme peak power of more than 10^{20} W/cm^2. Such x-ray pulses destroy samples in a single shot by a Coulomb explosion, forming a hot plasma or crater around the impact of the x-ray pulse in the case of liquids or solids. While the <10 femtoseconds (fs) pulse duration allows for interrogation of the intact sample before the destruction sets in (probe-before-destroy), the sample has to be replaced quickly before the arrival of the next pulse. XFELs operating with a warm copper linac at low repetition rates up to 120 Hz, including Linac Coherent Light Source (LCLS), SACLA, PAL-XFEL, and SwissFEL, permit relatively slow replenishment of sample material between pulses. Commonly used approaches include lateral translation for solid samples, jets at various speeds,[1,2] sometimes with an additional gas dynamic virtual nozzle (GDVN) focusing system (see, e.g., Refs. 3–9), and various forms of tape-drive droplet injectors.[10,11]

The much higher repetition rates obtained by XFEL pulse trains (10–30 ns pulse spacing) and at XFELs based on cryo-cooled linacs, such as at the European XFEL (EUXFEL) and LCLS-II, require a new approach to sample delivery. At very high repetition rates, replenishment becomes extremely challenging. For liquid jets, problems start to arise when the time between two consecutive pulses becomes smaller than 1 μs[12] due to, e.g., limitations of viscosity, Coulomb explosions inside the jet, and very high-speed rarefaction waves.[7,13,14] Even though the beam size can be very small (<1 μm), the effect of the explosion and the resulting plasma might extend tens of micrometers. For example, a 100 ns time spacing between pulses requires a jet speed of 100 m/s to move the sample by a modest value of 10 μm.

There is also an apparent practical problem with the high flow rates required for liquid jets to move at very high speeds, which may not be feasible given the cost of a pump capable of producing the jet and the availability of the sample. Finally, liquid subsonic jets are known to quickly develop turbulence shortly after leaving the nozzle and become highly collimated sprays, thus reducing the sample concentration.[15]

Solid-state samples are immune to most of these issues.[16] At low repetition rates, the delivery of small isolated samples, e.g., nanocrystals, has been achieved by raster scanning the samples using motion stages or tape drives.[10,17–21] At MHz or even higher repetition rates, and in cases where a large amount of low-cost sample is available, one can envision a different approach based on a fast-rotating disk. This work presents the results of consistently delivering a solid copper sample to the XFEL nanofocus with up to 60 m/s speed. This approach is potentially applicable for experiments where a large number of single-shot data is needed, such as serial femtosecond crystallography (SFX) or correlation x-ray fluorescence imaging (see, e.g., Ref. 22). While rotating samples have been employed previously (see, e.g., Ref. 23), the focus of the work presented here is on high-speed sample delivery.

We also point out a possible application of our system to deliver the gain medium in an x-ray laser oscillator (XLO) device. An XLO, as envisioned in Ref. 24, uses a train of XFEL pulses to pump a gain medium located inside a Bragg crystal optical cavity. The aim of the XLO is to generate high power, fully coherent, transform-limited hard x-ray pulses with improved stability when compared to XFEL pulses. Presently, an effort to demonstrate the first XLO is underway.[25,26] This proof-of-concept XLO will operate at the copper $K\alpha_1$ line, 8.05 keV, pumped by 9 keV XFEL pulses from the LCLS. In this configuration, the LCLS will deliver a train of pump pulses spaced at ~35 ns, a timing equivalent to the round trip of a 10 m cavity.[27,28] The ultra-high intensity XFEL pump pulses will transform any target material into a hot and rapidly expanding plasma, and rapid target replacement is crucial. For XLO gain media, the atomic density becomes important, and thus solid samples are favorable. For instance, it has been experimentally determined that the manageable concentration of the liquid copper nitrate jet is limited to 4M, which corresponds to the density of about 2 copper atoms/nm^3. In comparison, a solid copper foil has 80 atoms/nm^3. The increased atomic density can reduce the pump pulse intensity required to generate population inversion and, therefore, the area of damage to the sample.[15,29,30] Therefore, a rotating solid disk is the preferred method to deliver a gain medium or sample for experiments that have very high repetition rates, like the XLO. In this paper, we describe a rotating disk system using a solid 25 μm copper foil as a sample.

II. THEORETICAL CONSIDERATIONS

In this section, we discuss the required specifications for the sample delivery system including sample thickness and its variability, sample replacement speed, allowable axial oscillations, sample lifetime, and positional repeatability.

A. Positional control, sample speed, and lifetime

The high repetition rate x-ray pulse structure can be generalized in the following form. A number of pulses, n, is spaced by Δt, with a duty cycle defined by the machine trigger time T; see Fig. 1. Our system must deliver a fresh sample for each consecutive x-ray pulse. The required sample speed is therefore dictated by the x-ray repetition rate and the size of the damage crater the x-rays create. For instance, the approximate crater diameter left by the nanofocused x-rays in 25 μm copper foil is ~d = 20 μm for pulses of 45 μJ. Assuming a Gaussian focus with a diameter of 100 nm FWHM (50% of the photons fall within the FWHM) and a pulse length of 10 fs, this pulse energy corresponds to a peak intensity of $2.9 \cdot 10^{19}$ W/cm^2. At a 120 Hz repetition rate (such as available at LCLS), the minimum required linear velocity to clear the damage ($d/2$) is 1.2 mm/s, and the corresponding rotation frequency is $\nu_0 < 1$ rpm for a 150 mm diameter disk. In this case, a linear stage can also achieve this motion velocity. For the maximum repetition rate of 4.5 MHz experiments currently possible at the European XFEL, the corresponding linear and angular velocities are 45 m/s and ν_0 = 5730 rpm for a 150 mm disk. Finally, for XLO operations, with a pulse spacing of 35 ns, this gives a minimum target speed of ~286 m/s, a very high value close to the speed of sound in air, or ν_0 = 36 378 rpm for a 150 mm disk. We refer the reader to Table I for more use cases with different target damages.

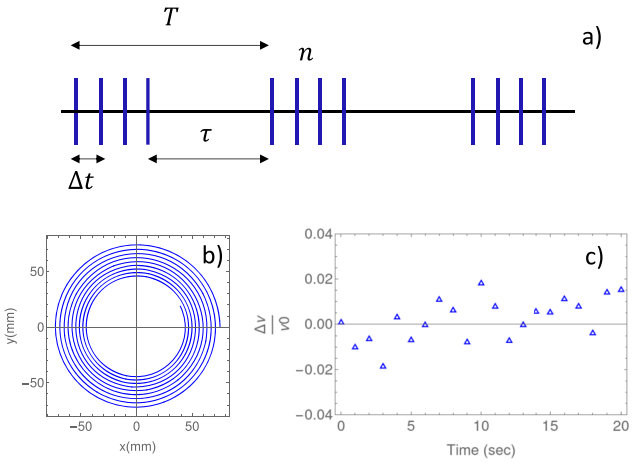

FIG. 1. (a) Generalized XFEL pulse timing structure: a pulse train of n pulses with spacing Δt is produced with a $1/T$ repetition rate. (b) Rastering trajectory on a 150 mm diameter solid sample. (c) Model angular velocity variations of the DC motor.

TABLE I. Attainable pulse spacing at various facilities LCLS in the multi-bunch (MB) mode, EUXFEL at max and nominal rates, LCLS-II, and corresponding target damage diameter, d, minimal linear velocity, and rotation frequency, v_{lin} and v_0, for replenishment in the case of a 150 mm rotating disk.

Δt (ns)	$1/\Delta t$ (MHz)	d (μm)	v_{lin} (m/s)	v_0 (rpm)	Comment
35	28.6	20	286	36 378	XLO@LCLS-MB
218	4.59	50	115	14 601	EUXFEL (max rate)
885	1.13	50	29	3 692	EUXFEL
1000	1.0	50	25	3 183	LCLS-II

The sample must move laterally to avoid exposing the same circumference on the disk for too long. The rastering trajectory on the sample can be described as a slowly converging (diverging) spiral:

$$x = r(t)\cos\,\phi(t),$$
$$y = r(t)\sin\,\phi(t), \tag{1}$$

where $r(t)$ is the distance from the center of the sample to the interaction point, $\phi(t) = \omega_0\, t + \int_0^t \Delta\omega(t')dt'$, and $\Delta\omega(t)$ is a random variation of the angular velocity (see Fig. 1).

For the pulse train structure shown in Fig. 1 and small variations of the rotation frequency, sufficient rotation speeds are needed to avoid strong overlap of the damage craters.

If the rotation frequency is a multiple of the inter-pulse frequency, all pulses from subsequent trains would irradiate the same small part of the disk circumference, resulting in a small sample coverage fraction. This is illustrated in Figs. 2(a) and 2(b), where the red color corresponds to the rotation frequency ν_0 = 3000 rpm, resulting in five turns of the disk between two successive trains. We assume a repetition rate $1/T$ = 10 Hz. If the rms relative variation of the rotation frequency is $\varepsilon = 10^{-4}$, then all pulse trains irradiate the same arc of the disk—close to the initial starting point—and thus, the effectiveness of the usage is dramatically decreased. If the rms is larger, e.g., 10^{-3}, as indicated by the blue arcs in Fig. 2(b), the random variations of the rotation speed lead to fluctuations in the number of turns between the trains, and thus the position of the irradiated arc spreads around the initial starting point. If the rms is increased further, e.g., 10^{-2}, as indicated by the gray arcs in Fig. 2(b), the accumulated spread of the position of the irradiated spot on the sample arc becomes so large that the position can be considered a random quantity. Figure 2(c) shows the case when the rotation frequency ν_0 = 3200 rpm, which corresponds to 5 $\frac{1}{3}$ turns. In this case, for a low variation of the rotation frequency, three consecutive pulse trains irradiate three arcs on the disk shifted by 1/3 of the turn. The subsequent pulse trains will irradiate the same three arcs where the material was damaged by the previous pulse trains. A similar situation takes place if the number of disk turns between trains is any rational number, thus leading to a fractal-like dependence of the covered fraction of the disk circumference on the repetition rate, as illustrated in Fig. 2(a). The sharp peaks in Fig. 2(a) that are close to the sharp dips correspond to the situation when the disk arc irradiated by one pulse train is situated next to an arc from a previous train—in this case, the whole disk circumference is fully used after time $T\frac{r}{\nu n\Delta t}$. When the fluctuation of the repetition rate is increased, the sharp drops and peaks of the covered fraction wash out and become less pronounced, especiallywhen arriving at the same position on the disk, which would require a large number of rotations. Further increasing the fluctuation of the rotation frequency results in the almost random placement of the irradiated arcs on the disk circumference; hence, the sharp dependence on the repetition rate disappears. In this case, one can estimate the covered sample fraction based on the following considerations: the increase in the fraction of the irradiated disk circumference c during time δt is proportional to the unirradiated part of the disk $1 - c$ and the arc fraction irradiated during time δt, namely $\nu\, n\Delta t\delta t/T$. This leads to

$$c(t) = 1 - e^{-\nu t\frac{n\Delta t}{T}}. \tag{2}$$

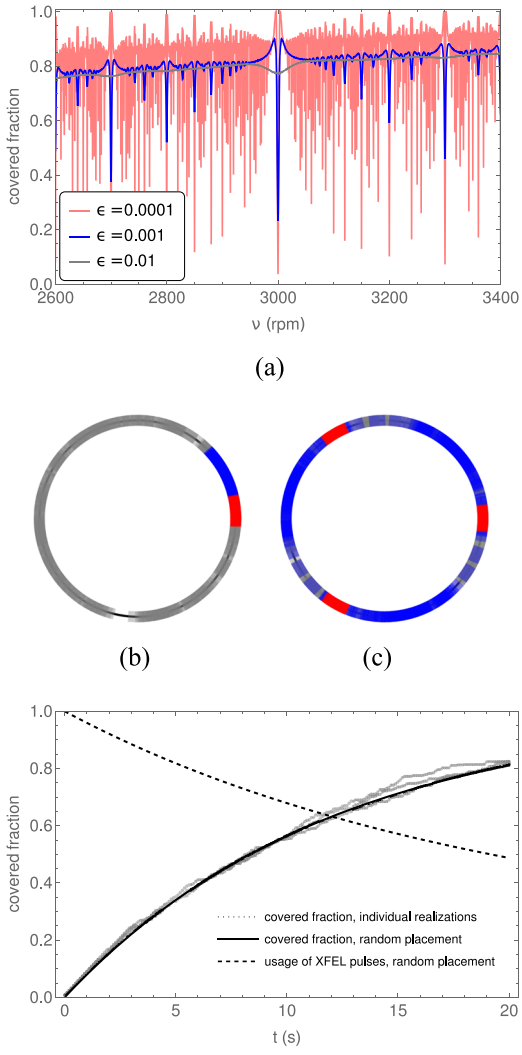

FIG. 2. Evolution of fraction of the irradiated disk circumference c for XFEL pulses sketched in Fig. 1(a), used parameters are $1/T$ = 10 Hz, n = 75, Δt = 2.1 μs. The time interval within which the rotation frequency is assumed to be constant [width of plateaus in Fig. 1(c)] is 0.5 s. (a) Dependence of the fraction of the irradiated disk circumference c on the rotation frequency ν after t = 20 s irradiation time for several rms variation of the rotation frequency $\varepsilon = \Delta\nu/\nu$. The plotted values are averaged over 5000 realizations of $\Delta\nu(t)$. (b) A single realization of disk irradiation at the parameters of Fig. (a) for the case ν = 3000 rpm. A thin black line shows the disk circumference, and different colors of arcs show the irradiated part of the circumferences for different values of ε. The same color coding as in Fig. (a) is used. (c) Same as Fig. (b) for the case ν = 3200 rpm. (d) Dependence of the irradiated part of the disk c on time for the case of ν = 3100 rpm. Gray dots show several individual realizations; the black solid line is an estimate according to Eq. (2); and the black dashed line shows the estimate of usage of XFEL pulses.

As Fig. 2(d) shows, Eq. (2) agrees well with the behavior for the case of 10^{-2} rms variation of the rotation frequency. Except for the short irradiation time, there is a probability of hitting the part of the disk circumference that was previously irradiated; therefore, the usage

of XFEL pulses [the ratio of the number of XFEL pulses that have irradiated the pristine part of the disk to the total number of XFEL pulses, $\frac{c(t)}{vtn\Delta t/T}$] is always smaller than one. It means that rotating targets will always naturally have some "bad" shots compared to, e.g., a sputtering source.[31] We note that the exact damage mechanism of solids and liquids from high-intensity x-ray pulses is a topic of active research and is not in the scope of this paper. Here, we have assumed that the pulse repetition rate $1/\Delta t$, crater size, and linear velocity are adjusted such that the disk arc—irradiated by one pulse train—is optimally used up, and this arc cannot be used once again for another train. In addition, the optimal value of the covered fraction of the disk circumference is a compromise between maximizing the amount of the used material and maintaining the mechanical integrity of the disk and should be decided for each experiment individually.

By intentionally modulating the speed of the motor in an aperiodic fashion about the nominal speed, we can ensure that the resonance is not hit with the light source frequency (i.e., a high effective ε is artificially achieved). A similar technique is employed by high-end lathes in order to mitigate "chatter," a problematic resonant interaction between the workpiece and the cutting tool.[32] However, since we need to consider longer relative time scales, a more carefully considered modulation is necessary. Specifically, by blending a range of anharmonic frequencies, we can effectively avoid resonances for the entire lifetime of each disk radius.

The typically required transverse positioning resolution is on the order of single micrometers, readily achievable with off-the-shelf screw-driven and piezo-driven positioning systems. The requirements for the linear stage speed are very low ($\ll$1 mm/s). We note that with the continuously spinning foil, it is challenging to associate individual damage spots with specific x-ray pulse intensities. Our system is primarily applicable to experiments where correlating the variations of the x-ray pulse intensities is not critical and/or the characterization of average conditions is sufficient. For saturated XFELs, the typical intensity fluctuation is about 30% rms.

B. Attenuation length of the sample and tolerances

In the case of thin metal foils, the typical thickness runs between 10 and 50 μm, depending on the attenuation length at a given wavelength. In cases where the attenuation length is a few μm long, the sample thickness should not vary by more than 10% across the sample in order to maintain similar x-ray absorption conditions. We note that, for instance, off-the-shelf copper and aluminum foil thickness profiles were measured at the Stanford Synchrotron Radiation Lightsource (SSRL) and were found to have thickness variations below the 5% level.

In experiments where the target is precisely placed in the x-ray focus, it must also not deviate excessively from the focal point. In other words, the allowed amount of axial oscillation amplitude should be less than the Rayleigh range of the focused x-rays. For instance, in the case of XLO, the stringent requirement of the nanofocus limits the allowable offset to ~±30 μm (see Fig. 3).

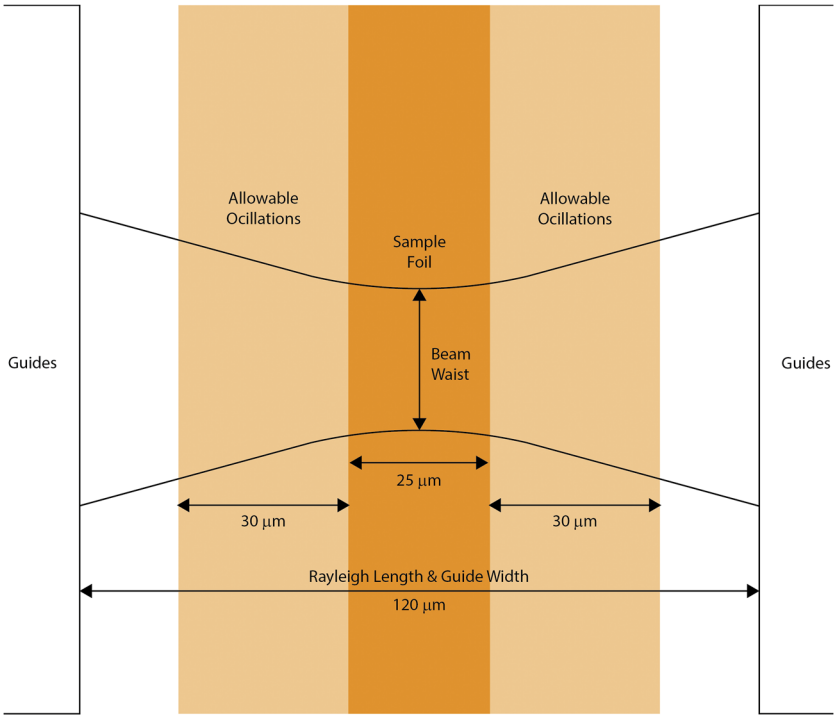

FIG. 3. Diagram showing the nano-focused x-ray beam envelope, the guides, and allowable foil oscillations.

C. Other considerations

As the x rays are appreciably scattered by air, the sample should be placed in a helium atmosphere or under a vacuum. It is necessary that the sample delivery system can work under both conditions for the duration of the experiment. Helium has the added benefit of a much higher speed of sound (927 m/s) than air (344 m/s), which allows the sample to move faster without being transonic or supersonic, avoiding instabilities associated with these regimes. Low vacuum is easily attained by adding a vacuum roughing pump, which will remove any drag forces that may cause instabilities during the sample rotation. High vacuum can be attained with modifications to the system for cooling and reducing out-gassing.

III. EXPERIMENTAL SETUP AND VALIDATION

This section presents the results of our laboratory measurements while designing and building the prototype in the lab and the subsequent experiments at the LCLS-CXI and European XFEL SPB/SFX beamlines.[33,34] We first built and commissioned a spinning-disk system using a DC motor system for operations at LCLS. We tested the sample stability along the beam direction at various speeds and characterized the size of the craters resulting from the impact of each XFEL pulse. The crater size depends on the XFEL pulse intensity and, together with the repetition rate, it defines the required speed when operating the spinning disk as either the gain medium target or for sample delivery.

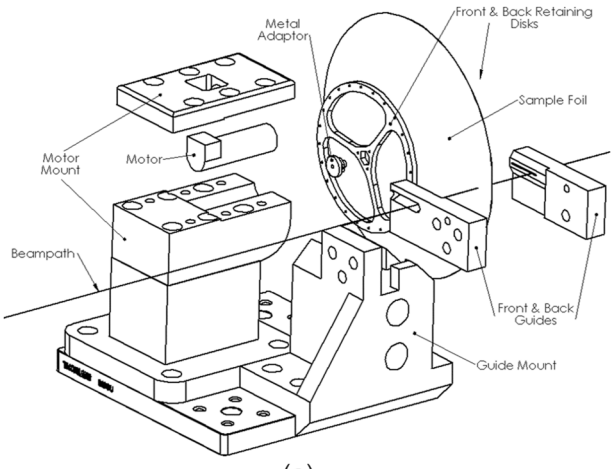

(a)

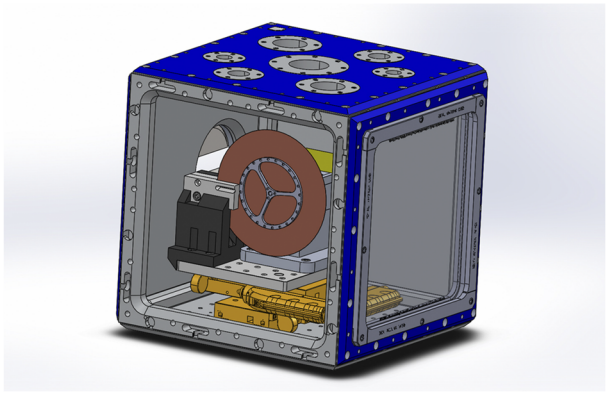

(b)

FIG. 4. (Top) Exploded diagram of the DC-motor sample delivery system. (Bottom) CAD model of the sample delivery system integrated into the vacuum chamber (with the front panel removed).

A. DC-motor system

Our DC-motor system used a direct drive rotor where a foil is directly mounted onto the motor axis; see Fig. 4. Utilizing a small and efficient DC motor (Assun AM-BL1640AN-1816) minimizes vibrations generated by the system. A 3D-printed carbon fiber reinforced nylon frame retains the foil, acting as an adapter and allowing for quickly swapping foils. To keep the foil stable along the beam axis, we constrain the foil oscillations at the XFEL pulse interaction point with a PTFE (Teflon) guide that limits the oscillations while minimizing friction between the moving foil and itself. Foils were 150 mm in diameter and 25 μm in thickness. After mounting in the carbon fiber frame, the copper disk weighs ~20 g, and the system could, in theory, accept disks up to 100 g without significant losses in performance. Guide width varied between 150 and 250 μm, corresponding to the desired Raleigh length of the nano-focused x-ray beam. The entire system has a footprint of 6 × 8 × 7 in.^{3} and is assembled on a single breadboard to reduce the required alignment.

To characterize the stability of the systems along the x-ray beam direction (parallel to the disk rotation axes), a commercial laser Doppler vibrometer (Optomet, SWIR vibrometer) was employed. For this, the direct drive system was set up with a 250 μm guide, and the vibrometer was directed into the guide at a radial distance of about 125 mm. Displacement measurements taken at three different common rotation speeds over 0.5 s are shown in Fig. 5. While there are oscillations on or below the order of rotation speed, long-term drift is limited due to the physical boundary condition imposed by the guide and is more dependent on the stability of the chamber in which the system is mounted. The baseline vibrations of the DC motor assembly at 1000 rpm were measured to be 3 μm p–p at a frequency of about 13 Hz, indicating some disturbance to the mounting of the experimental apparatus. A disruption of rotation from the XFEL pulse impact was tested with an optical system in the laboratory. This system was hit by a focused 400 nm laser pulse, which ablated small craters similar to what was expected at LCLS. Our tests revealed few perturbations to the target.

The direct drive system carrying a copper foil disk was then deployed at the CXI user end station at LCLS, configured in nano-focus mode. Operating as part of the XLO cavity validation, the system was able to replenish copper at the focus to produce K_α radiation to calibrate the cavity detector and initial XLO cavity crystal alignment [see Fig. 6(a)]. A lifetime of about 8 h/disk was achieved with roughly 90% of sample consumption.

We then proceeded to deploy our system in a high vacuum scattering experiment at EUXFEL. In this experiment, the pristine copper foil was coated with molecules of interest, and the guides were modified for scattering angle allowances. Once at high vacuum and thermal equilibrium, the motor was able to accelerate up to 3000 rpm consistently and operate in this regime. The coated foil was

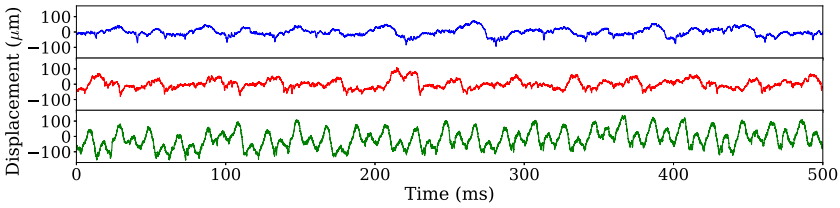

FIG. 5. Laser Doppler vibrometer displacement measurements at 1000 rpm, with the rms oscillation of 25.6 μm (top trace); at 1500 rpm, with the rms oscillation of 33.8 μm (middle trace), and at 3000 rpm, with the rms oscillation of 55.5 μm (bottom trace).

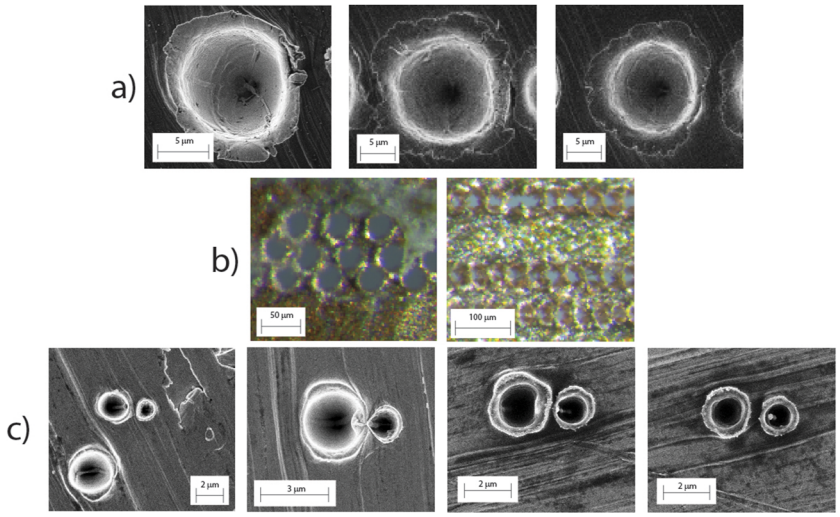

FIG. 6. (a) Single craters produced by LCLS 9 keV 20 μJ pulses in copper in nominal 120 Hz mode. (b) Optical microscopy images of the craters produced with 9 keV 50 μJ pulses at European XFEL with the copper disk running at 3000 rpm. (c) SEM measurements of copper craters resulting from two 9 keV 10 μJ LCLS x-ray pulses spaced by 35 ns resulting in a 2.1 μm spacing at a sample speed of 60 m/s.

sampled at varying speeds and successfully operated consistently at a half-MHz sampling rate with short sampling periods at 1.13 MHz due to shorter foil lifetimes. A typical crater pattern on a copper foil is shown in Fig. 6(b). Therefore, we conclude that our setup can be readily used for other high repetition x-ray experiments at LCLS, EUXFEL, or elsewhere.

B. Air spindle system tests

We have also tested an air spindle-based high-speed delivery system. It employed an air turbine motor driving a high-speed spindle connected to the same foil frame style used for the DC motor. The turbine motor can be driven by compressed air or helium gas to speeds between 200 and 400 m/s (30 000–60 000 rpm). The high speed helps axial stability as the centrifugal forces tend toward planar motion. With this system, we have achieved a sample velocity of up to 60 m/s (7600 rm) and tested it with the LCLS bunch train operation, delivering two pulses separated by 35 ns.[27] The resulting craters are shown in Fig. 6(c), confirming the target moved fast enough to resolve two consecutive pulses in a 35 ns pulse train. We note that mutual x-ray intensity fluctuations from LCLS in two-pulse mode result in different double crater sizes. However, the air spindle system exhibited large axial oscillations, resulting in displacements along the beam direction averaging ~500 μm peak to peak. Operation of an air spindle system will require engineering upgrades that address these oscillations before it will be feasible for operations at nanofocus XFEL experiments, which typically have a Rayleigh length of 120 μm.

IV. TARGET UPGRADE AND FUTURE SPINDLE DEVELOPMENT

To further advance our solid target setup, we are developing an upgraded target system for even higher speeds, greater stability, and improved longevity. This system will have two main distinctions from the implementations already discussed: the first is the use of a rigid pair of retaining disks to tension and support the foil, and the second is employing a dedicated spindle system to minimize oscillations of the rotor and thus foil (Fig. 7). The use of robust retaining disks dramatically reduces the demands placed on the mechanical properties of the foil itself; instead, these retaining disks can be fabricated to very tight tolerances using machining processes like wire electrical discharge machining (EDM) and precision grinding. This also means that the range of candidate foil materials can be

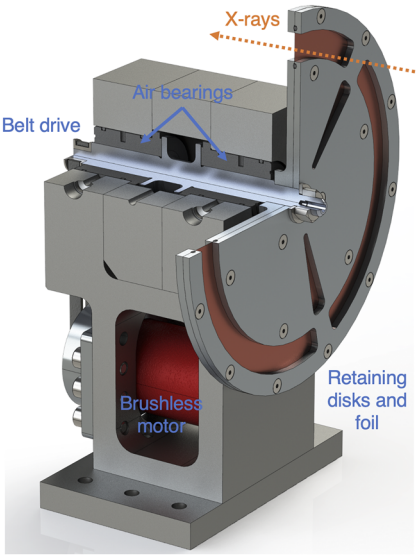

FIG. 7. Annotated schematic of the upgraded target system using air bearings and rigid retaining disks.

significantly expanded. The robustness and repeatability of this approach are quantified by some of the measurements below. Moreover, since the spinning foil no longer needs to contact other objects, the likelihood of catastrophic failure is substantially reduced, especially for extended run times at high speed. This lack of contact is especially valuable for scenarios where a thin layer of sample is deposited onto a foil substrate, which would be susceptible to damage by fixed guides. This approach, however, does come with challenges. The rotating mass is many times larger, requiring a far more stringent design of the target system in addition to a more powerful motor. Furthermore, a retaining disk with spokes, as the present design uses, does occlude some of the target material (~8% in this case).

Two different spindle systems are being developed in parallel. One employs air bearings pressurized by helium, as shown in Fig. 7, while the other uses high precision ball bearings in a similar configuration. Air bearings offer much lower friction and superb radial and axial alignment but have a much lower tolerance for both static and dynamic imbalances in the rotor and disk.

The mechanical bearing system was characterized using the same laser Doppler vibrometer system at a range of speeds in helium at atmospheric pressure. In each case, the system was set to a target speed and allowed to settle before the rms vibration was measured (Fig. 8). In contrast with the unsupported foil, the vibrations did not tend to increase at higher speeds; if anything, the trend was improving as the centrifugal force effectively stiffened the retaining disks. Future tests in vacuum are anticipated to reduce the vibrations even further.

To supplement these measurements, the air-bearing-based target was also characterized using a confocal displacement sensor,[35] which measures the absolute axial displacement of the foil. The deviation of the foil from a perpendicular plane was inferred (Fig. 9).

After the target was allowed to stabilize at 4800 rpm, the foil's axial position was measured for 12 000 revolutions. Using the sharp edges associated with the spokes, the data for all 12 000 turns were aligned, and the mean and standard deviation at each angular position were recorded (Fig. 9). The small error bars illustrate the excellent turn-to-turn stability of the system: the axial position of the foil as a function of the angle is extremely reproducible. This indicates that a flat retaining disk will consistently deliver flat foil without appreciable vibration or aerodynamic flutter.

Our sample delivery systems can also benefit laser ablation experiments with an optical laser pump and x-ray probe. In these types of experiments, linear translation stages are commonly used, limiting the repetition rate of the experiment due to the need to replenish the relatively large, damaged region of the sample. For instance, typical laser ablated craters in copper are shown in Fig. 10. In this case, a 1064 nm Nd:YAG laser with 77 mJ pulse energy was

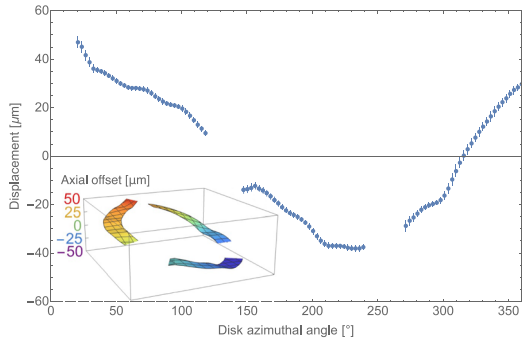

FIG. 9. Confocal displacement sensor data from 12 000 revolutions of the air bearing target system. Error bars are the standard deviation. (Inset) Inferred map of the axial offset of the foil as measured by the confocal displacement sensor (not to scale).

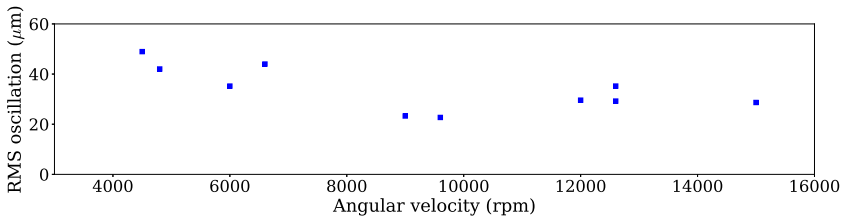

FIG. 8. Laser Doppler vibrometer measurements of the mechanical bearing target foil vibration as a function of angular velocity.

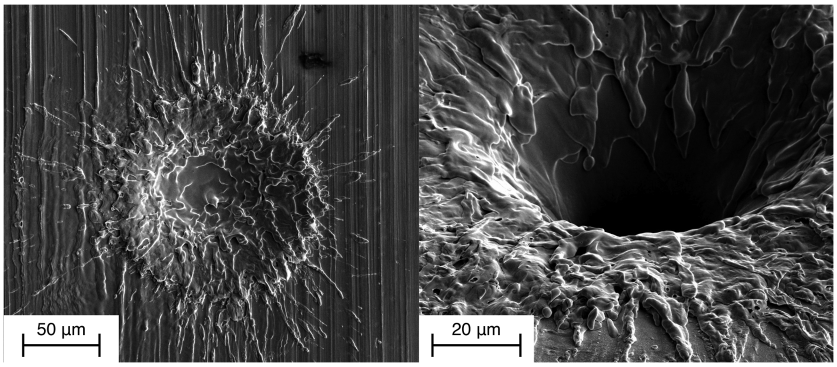

FIG. 10. Example SEM images of optically ablated craters in copper using a Nd:YAG 1064 nm laser with 77 mJ pulses. (Left) The foil was not at the focal point, reducing the intensity. (Right) The foil is close to the focal point, and the 25 μm foil is completely punctured.

employed. Using the fast rotating target, we can increase the data collection rate in these types of experiments. One can also investigate the recoil effects of the plasma plume on the target using optical laser ablation. We have begun to develop a testing protocol using an Nd:YAG infrared laser to enable testing without requiring access to an x-ray beamline.

V. SUMMARY

In summary, we have demonstrated a continuous solid target sample delivery system capable of operating at high-repetition-rate x-ray sources. We have studied its performance as an XFEL target using a 25 μm copper foil in a helium atmosphere and in vacuum. We envision the use of other foils made of different materials (e.g., low absorbing plastic films) and comparable thicknesses in various user experiments. This approach could become applicable for the rapid delivery of many systems continuously dispensed on the rotating disk, including proteins or nanocrystals. Finally, we validated the mechanical design of the direct drive variable speed system capable of accelerating the copper foil up to 36 000 rpm. The results of this development will be published in the future.

ACKNOWLEDGMENTS

This work was supported by DOE Grant Nos. DE-SC0009914, DE-AC02-76SF00515, and DE-SC-0023585. The authors would like to acknowledge D. De-Ponte, M. Liang, S. Boutet (SLAC, USA), J. Bielecki, A. Round, J. Koliyadu, P. Vagovic (European XFEL, Germany), and T. Ban (Vibrations, Inc., USA) for their help with the system validation at the LCLS and European XFEL facilities. We acknowledge European XFEL in Schenefeld, Germany, for the provision of x-ray free-electron laser beamtime at Scientific Instrument SPB/SFX (Single Particles, Clusters, and Biomolecules and Serial Femtosecond Crystallography) and would like to acknowledge the staff for their assistance.

AUTHOR DECLARATIONS

Conflict of Interest

The authors have no conflicts to disclose.

Author Contributions

N.W. and N.M. contributed equally to this work.

N. Welke: Formal analysis (equal); Investigation (equal); Methodology (equal); Validation (equal); Writing – original draft (equal). **N. Majernik**: Conceptualization (equal); Data curation (equal); Formal analysis (equal); Investigation (equal); Methodology (equal); Software (equal); Supervision (equal); Validation (equal); Visualization (equal); Writing – original draft (equal); Writing – review & editing (equal). **R. Ash**: Resources (equal); Validation (equal). **A. Moro**: Conceptualization (equal); Data curation (equal); Formal analysis (equal); Investigation (equal); Methodology (equal); Resources (equal); Software (equal); Validation (equal). **R. Agustsson**: Conceptualization (equal); Investigation (equal); Methodology (equal); Project administration (equal); Resources (equal). **P. Manwani**: Data curation (equal); Formal analysis (equal); Investigation (equal). **K. Li**: Formal analysis (equal); Investigation (equal); Methodology (equal). **A. Sakdinawat**: Formal analysis (equal); Methodology (equal); Resources (equal). **A. Aquila**: Formal analysis (equal); Investigation (equal); Methodology (equal); Supervision (equal); Validation (equal). **A.1 Benediktovitch**: Conceptualization (equal); Formal analysis (equal); Investigation (equal); Visualization (equal). **A.1 Halavanau**: Conceptualization (equal); Formal analysis (equal); Investigation (equal); Methodology (equal); Supervision (equal); Writing – review & editing (equal). **J.1 Rosenzweig**: Conceptualization (equal); Investigation (equal); Methodology (equal); Project administration (equal); Resources (equal); Supervision (equal). **U.1 Bergmann**: Conceptualization (equal); Formal analysis (equal); Investigation (equal); Methodology (equal); Project administration (equal); Resources (equal); Supervision (equal); Visualization (equal); Writing – original draft (equal). **C.1 Pellegrini**: Conceptualization (equal); Formal analysis (equal); Investigation (equal); Methodology (equal); Project administration (equal); Resources (equal); Supervision (equal); Validation (equal); Writing – original draft (equal).

DATA AVAILABILITY

The experimental data for this study are available from the corresponding authors upon reasonable request.

REFERENCES

[1]R. G. Sierra, H. Laksmono, J. Kern, R. Tran, J. Hattne, R. Alonso-Mori, B. Lassalle-Kaiser, C. Glöckner, J. Hellmich, D. W. Schafer *et al.*, "Nanoflow electrospinning serial femtosecond crystallography," Acta Crystallogr., Sect. D: Biol. Crystallogr. **68**, 1584–1587 (2012).

[2]U. Weierstall, D. James, C. Wang, T. A. White, D. Wang, W. Liu, J. C. Spence, R. Bruce Doak, G. Nelson, P. Fromme *et al.*, "Lipidic cubic phase injector facilitates membrane protein serial femtosecond crystallography," Nat. Commun. **5**, 3309 (2014).

[3]A. M. Gañán Calvo, "Generation of steady liquid microthreads and micron-sized monodisperse sprays in gas streams," Phys. Rev. Lett. **80**, 285–288 (1998).

[4]D. P. DePonte, U. Weierstall, K. Schmidt, J. Warner, D. Starodub, J. C. H. Spence, and R. B. Doak, "Gas dynamic virtual nozzle for generation of microscopic droplet streams," J. Phys. D: Appl. Phys. **41**, 195505 (2008).

[5]A. Doerr, "Diffraction before destruction," Nat. Methods **8**, 283 (2011).

[6]H. N. Chapman, C. Caleman, and N. Timneanu, "Diffraction before destruction," Philos. Trans. R. Soc., B **369**, 20130313 (2014).

[7]M. L. Grünbein, A. Gorel, L. Foucar, S. Carbajo, W. Colocho, S. Gilevich, E. Hartmann, M. Hilpert, M. Hunter, M. Kloos, J. E. Koglin, T. J. Lane, J. Lewandowski, A. Lutman, K. Nass, G. Nass Kovacs, C. M. Roome, J. Sheppard, R. L. Shoeman, M. Stricker, T. van Driel, S. Vetter, R. B. Doak, S. Boutet, A. Aquila, F. J. Decker, T. R. M. Barends, C. A. Stan, and I. Schlichting, "Effect of x-ray free-electron laser-induced shockwaves on haemoglobin microcrystals delivered in a liquid jet," Nat. Commun. **12**, 1672 (2021).

[8]R. G. Sierra, U. Weierstall, D. Oberthuer, M. Sugahara, E. Nango, S. Iwata, and A. Meents, "Sample delivery techniques for serial crystallography," in *X-Ray Free Electron Lasers: A Revolution in Structural Biology*, edited by S. Boutet, P. Fromme, and M. S. Hunter (Springer International Publishing, Cham, 2018), pp. 109–184.

[9]U. Weierstall, J. Spence, and R. Doak, "Injector for scattering measurements on fully solvated biospecies," Rev. Sci. Instrum. **83**, 035108 (2012).

[10]F. D. Fuller, S. Gul, R. Chatterjee, E. S. Burgie, I. D. Young, H. Lebrette, V. Srinivas, A. S. Brewster, T. Michels-Clark, J. A. Clinger, B. Andi, M. Ibrahim, E. Pastor, C. de Lichtenberg, R. Hussein, C. J. Pollock, M. Zhang, C. A. Stan, T. Kroll, T. Fransson, C. Weninger, M. Kubin, P. Aller, L. Lassalle, P. Bräuer, M. D. Miller, M. Amin, S. Koroidov, C. G. Roessler, M. Allaire, R. G. Sierra, P. T. Docker, J. M. Glownia, S. Nelson, J. E. Koglin, D. Zhu, M. Chollet, S. Song, H. Lemke, M. Liang, D. Sokaras, R. Alonso-Mori, A. Zouni, J. Messinger, U. Bergmann, A. K. Boal, J. M. Bollinger, C. Krebs, M. Högbom, G. N. Phillips, R. D. Vierstra, N. K. Sauter, A. M. Orville, J. Kern, V. K. Yachandra, and J. Yano, "Drop-on-demand sample delivery for studying biocatalysts in action at x-ray free-electron lasers," Nat. Methods **14**, 443–449 (2017).

[11]A. Henkel, J. Maracke, A. Munke, M. Galchenkova, A. Rahmani Mashhour, P. Reinke, M. Domaracky, H. Fleckenstein, J. Hakanpää, J. Meyer *et al.*, "CFEL TapeDrive 2.0: A conveyor belt-based sample-delivery system for multi-dimensional serial crystallography," Acta Crystallogr., Sect. A: Found. Adv. **78**, a560 (2022).

[12]P. Abbamonte, F. Abild-Pedersen, P. Adams, M. Ahmed, F. Albert, R. A. Mori, P. Anfinrud, A. Aquila, M. Armstrong, J. Arthur, J. Bargar, A. Barty, U. Bergmann, N. Berrah, G. Blaj, H. Bluhm, C. Bolme, C. Bostedt, S. Boutet, G. Brown, P. Bucksbaum, M. Cargnello, G. Carini, A. Cavalleri, V. Cherezov, W. Chiu, Y. Chuang, D. Cocco, R. Coffee, G. Collins, A. Cordones-Hahn, J. Cryan, G. Dakovski, M. Dantus, H. Demirci, P. Denes, T. Devereaux, Y. Ding, S. Doniach, R. Dorner, M. Dunne, H. Durr, T. Egami, D. Eisenberg, P. Emma, C. Fadley, R. Falcone, Y. Feng, P. Fischer, F. Fiuza, L. Fletcher, L. Foucar, M. Frank, J. Fraser, H. Frei, D. Fritz, P. Fromme, A. Fry, M. Fuchs, P. Fuoss, K. Gaffney, E. Gamboa, O. Gessner, S. Ghimire, A. Gleason, S. Glenzer, T. Gorkhover, A. Gray, M. Guehr, J. Guo, J. Hajdu, S. Hansen, P. Hart, M. Hashimoto, J. Hastings, D. Haxton, P. Heimann, T. Heinz, A. Hexemer, J. Hill, F. Himpsel, P. Ho, B. Hogue, Z. Huang, M. Hunter, G. Hura, N. Huse, Z. Hussain, M. Ilchen, C. Jacobsen, C. Kenney, J. Kern, S. Kevan, J. Kim, H. Kim, P. Kirchmann, R. Kirian, S. Kivelson, C. Kliewer, J. Koralek, G. Kovacsova, A. Lanzara, J. LaRue, H. Lee, J. Lee, W. Lee, Y. Lee, I. Lindau, A. Lindenberg, Z. Liu, D. Lu, U. Lundstrom, A. MacDowell, W. Mao, J. Marangos, G. Marcus, T. Martinez, W. McCurdy, G. McDermott, C. McGuffey, M. Minitti, S. Miyabe, S. Moeller, R. Moore, S. Mukamel, K. Nass, A. Natan, K. Nelson, S. Nemsak, D. Neumark, R. Neutze, A. Nilsson, D. Nordlund, J. Norskov, S. Nozawa, H. Ogasawara, H. Ohldag, A. Orville, D. Osborn, T. Osipov, A. Ourmazd, D. Parkinson, C. Pellegrini, G. Phillips, T. Rasing, T. Raubenheimer, T. Recigno, A. Reid, D. Reis, A. Robert, J. Robinson, D. Rolles, J. Rost, S. Roy, A. Rudenko, T. Russell, R. Sandberg, A. Sandhu, N. Sauter, I. Schlichting, R. Schlogl, W. Schlotter, M. Schmidt, J. Schneider, R. Schoenlein, M. Schoeffler, A. Scholl, Z. Shen, O. Shpyrko, T. Silva, S. Sinha, D. Slaughter, J. Sobota, D. Sokaras, K. Sokolowski-Tinten, S. Southworth, J. Spence, C. Stan, J. Stohr, R. Stroud, V. Sundstrom, C. Taatjes, A. Thomas, M. Trigo, Y. Tsui, J. Turner, A. van Buuren, S. Vinko, S. Wakatsuki, J. Wark, P. Weber, T. Weber, M. Wei, T. Weiss, P. Wernet, W. White, P. Willmott, K. Wilson, W. Wurth, V. Yachandra, J. Yano, D. Yarotski, L. Young, Y. Zhu, D. Zhu, and P. Zwart, "New science opportunities enabled by LCLS-II x-ray lasers," Technical Report (2015).

[13]C. A. Stan, D. Milathianaki, H. Laksmono, R. G. Sierra, T. McQueen, M. Messerschmidt, G. J. Williams, J. E. Koglin, T. J. Lane, M. Hayes, S. A. H. Guillet, M. Liang, A. L. Aquila, P. R. Willmott, J. Robinson, K. L. Gumerlock, S. Botha, K. Nass, I. Schlichting, R. Shoeman, H. A. Stone, and S. Boutet, "Liquid explosions induced by x-ray laser pulses," Nat. Phys. **12**, 966–971 (2016).

[14]F. Perakis, G. Camisasca, T. J. Lane, A. Späh, K. T. Wikfeldt, J. A. Sellberg, F. Lehmkühler, H. Pathak, K. H. Kim, K. Amann-Winkel, S. Schreck, S. Song, T. Sato, M. Sikorski, A. Eilert, T. McQueen, H. Ogasawara, D. Nordlund, W. Roseker, J. Koralek, S. Nelson, P. Hart, R. Alonso-Mori, Y. Feng, D. Zhu, A. Robert, G. Grübel, L. G. M. Pettersson, and A. Nilsson, "Coherent x-rays reveal the influence of cage effects on ultrafast water dynamics," Nat. Commun. **9**, 1917 (2018).

[15]M. Yadav, E. Galtier, A. Halavanau, N. Majernik, A. Malinouski, P. Manwani, B. Naranjo, C. Pellegrini, and J. Rosenzweig, "Optimization of the gain medium delivery system for an X-ray laser oscillator," in *IPAC2021, MOPAB150*, 2021, http://www.jacow.org.

[16]A. Žemaitis, P. Gečys, M. Barkauskas, G. Račiukaitis, and M. Gedvilas, "Highly-efficient laser ablation of copper by bursts of ultrashort tuneable (fs-ps) pulses," Sci. Rep. **9**, 12280 (2019).

[17]P. Zalden, F. Quirin, M. Schumacher, J. Siegel, S. Wei, A. Koc, M. Nicoul, M. Trigo, P. Andreasson, H. Enquist, M. J. Shu, T. Pardini, M. Chollet, D. Zhu, H. Lemke, I. Ronneberger, J. Larsson, A. M. Lindenberg, H. E. Fischer, S. Hau-Riege, D. A. Reis, R. Mazzarello, M. Wuttig, and K. Sokolowski-Tinten, "Femtosecond x-ray diffraction reveals a liquid–liquid phase transition in phase-change materials," Science **364**, 1062–1067 (2019).

[18]A. Meents, M. O. Wiedorn, V. Srajer, R. Henning, I. Sarrou, J. Bergtholdt, M. Barthelmess, P. Y. A. Reinke, D. Dierksmeyer, A. Tolstikova, S. Schaible, M. Messerschmidt, C. M. Ogata, D. J. Kissick, M. H. Taft, D. J. Manstein, J. Lieske, D. Oberthuer, R. F. Fischetti, and H. N. Chapman, "Pink-beam serial crystallography," Nat. Commun. **8**, 1281 (2017).

[19]P. Roedig, H. M. Ginn, T. Pakendorf, G. Sutton, K. Harlos, T. S. Walter, J. Meyer, P. Fischer, R. Duman, I. Vartiainen, B. Reime, M. Warmer, A. S. Brewster, I. D. Young, T. Michels-Clark, N. K. Sauter, A. Kotecha, J. Kelly, D. J. Rowlands, M. Sikorsky, S. Nelson, D. S. Damiani, R. Alonso-Mori, J. Ren, E. E. Fry, C. David, D. I. Stuart, A. Wagner, and A. Meents, "High-speed fixed-target serial virus crystallography," Nat. Methods **14**, 805–810 (2017).

[20]S. Oghbaey, A. Sarracini, H. M. Ginn, O. Pare-Labrosse, A. Kuo, A. Marx, S. W. Epp, D. A. Sherrell, B. T. Eger, Y. Zhong, R. Loch, V. Mariani, R. Alonso-Mori, S. Nelson, H. T. Lemke, R. L. Owen, A. R. Pearson, D. I. Stuart, O. P. Ernst, H. M. Mueller-Werkmeister, and R. J. D. Miller, "Fixed target combined with spectral mapping: Approaching 100% hit rates for serial crystallography," Acta Crystallogr., Sect. D: Struct. Biol. **72**, 944–955 (2016).

[21]R. Alonso-Mori, D. Sokaras, M. Cammarata, Y. Ding, Y. Feng, D. Fritz, K. J. Gaffney, J. Hastings, C.-C. Kao, H. T. Lemke, T. Maxwell, A. Robert, A. Schropp, F. Seiboth, M. Sikorski, S. Song, T.-C. Weng, W. Zhang, S. Glenzer, U. Bergmann, and D. Zhu, "Femtosecond electronic structure response to high intensity XFEL pulses probed by iron x-ray emission spectroscopy," Sci. Rep. **10**, 16837 (2020).

[22]F. Trost, K. Ayyer, M. Prasciolu, H. Fleckenstein, M. Barthelmess, O. Yefanov, J. L. Dresselhaus, C. Li, S. c. v. Bajt, J. Carnis, T. Wollweber, A. Mall, Z. Shen, Y. Zhuang, S. Richter, S. Karl, S. Cardoch, K. K. Patra, J. Möller, A. Zozulya, R. Shayduk, W. Lu, F. Brauße, B. Friedrich, U. Boesenberg, I. Petrov, S. Tomin, M. Guetg, A. Madsen, N. Timneanu, C. Caleman, R. Röhlsberger, J. von Zanthier, and

H. N. Chapman, "Imaging via correlation of x-ray fluorescence photons," Phys. Rev. Lett. **130**, 173201 (2023).
[23]I. Martiel, H. M. Müller-Werkmeister, and A. E. Cohen, "Strategies for sample delivery for femtosecond crystallography," Acta Crystallogr., Sect. D: Struct. Biol. **75**, 160–177 (2019).
[24]A. Halavanau, A. Benediktovitch, A. A. Lutman, D. DePonte, D. Cocco, N. Rohringer, U. Bergmann, and C. Pellegrini, "Population inversion x-ray laser oscillator," Proc. Natl. Acad. Sci. U. S. A. **117**, 15511–15516 (2020).
[25]A. Halavanau, R. Alonso-Mori, A. Aquila, U. Bergmann, D. DePonte, F.-J. Decker, M. Doyle, F. Fuller, M. Liang, A. Lutman, and C. Pellegrini, "Progress report on population inversion-based x-ray laser oscillator," in *Proceedings of IPAC'21, International Particle Accelerator Conference No. 12*, Geneva, Switzerland, 2021, http://www.jacow.org, pp. 373–375.
[26]A. Halavanau, R. Alonso-Mori, A. Aquila, R. Ash, A. I. Benediktovitch, U. Bergmann, F. J. Decker, F. Fuller, S. C. Krusic, M. Liang, A. A. Lutman, N. Majernik, P. Manwani, R. A. Margraf, R. H. Paul, C. Pellegrini, R. Robles, N. Rohringer, J. B. Rosenzweig, and N. B. Welke, "Progress report on population inversion x-ray laser oscillator at LCLS," in *Proceedings of IPAC 2022, Bangkok, Thailand* (2022).
[27]F.-J. Decker, K. L. Bane, W. Colocho, S. Gilevich, A. Marinelli, J. C. Sheppard, J. L. Turner, J. J. Turner, S. L. Vetter, A. Halavanau, C. Pellegrini, and A. A. Lutman, "Tunable x-ray free electron laser multi-pulses with nanosecond separation," Sci. Rep. **12**, 3253 (2022).
[28]A. Halavanau, A. Romero, A. Krasnykh, A. Lutman, T. Beukers, J. Hugyik, A. Le, K. Luchini, E. Jongewaard, A. Sy, A. Ibrahimov, A. Benwell, A. Marinelli, and F.-J. Decker, "Ultra-fast transverse beam orbit control in LCLS copper linac. Part I," J. Instrum. **17**, P11031 (2022).
[29]P. Manwani, E. Galtier, A. Halavanau, N. Majernik, B. Naranjo, C. Pellegrini, and J. Rosenzweig, "Modelling of x-ray volume excitation of the XLO gain medium using flash," International Particle Accelerator Conference, TUPOPT034, 2022.
[30]N. Majernik, R. B. Agustsson, R. Ash, U. Bergmann, A. Halavanau, N. Inzunza, P. Manwani, A. Moro, C. Pellegrini, J. B. Rosenzweig, and N. B. Welke, "Foiled again: Solid-state sample delivery for high repetition rate XFELs," in *Proceedings of IPAC 2022, Bangkok, Thailand* (2022).
[31]Q. L. D. Nguyen, J. Simoni, K. M. Dorney, X. Shi, J. L. Ellis, N. J. Brooks, D. D. Hickstein, A. G. Grennell, S. Yazdi, E. E. B. Campbell, L. Z. Tan, D. Prendergast, J. Daligault, H. C. Kapteyn, and M. M. Murnane, "Direct observation of enhanced electron-phonon coupling in copper nanoparticles in the warm-dense matter regime," Phys. Rev. Lett. **131**, 085101 (2023) .
[32]T. Takemura, T. Kitamura, and T. Hoshi, "Active suppression of chatter by programed variation of spindle speed," Memoirs of the Faculty of Engineering, Kyoto University, 1975, Vol. 37, pp. 62–76.
[33]S. Boutet and G. J. Williams, "The coherent x-ray imaging (CXI) instrument at the linac coherent light source (LCLS)," New J. Phys. **12**, 035024 (2010).
[34]J. C. P. Koliyadu, R. Letrun, H. J. Kirkwood, J. Liu, M. Jiang, M. Emons, R. Bean, V. Bellucci, J. Bielecki, S. Birnsteinova, R. de Wijn, T. Dietze, J. E, J. Grünert, D. Kane, C. Kim, Y. Kim, M. Lederer, B. Manning, G. Mills, L. L. Morillo, N. Reimers, D. Rompotis, A. Round, M. Sikorski, C. M. S. Takem, P. Vagovič, S. Venkatesan, J. Wang, U. Wegner, A. P. Mancuso, and T. Sato, "Pump–probe capabilities at the SPB/SFX instrument of the European XFEL," J. Synchrotron Radiat. **29**, 1273–1283 (2022).
[35]Confocal displacement sensor—CL-3000 series, https://www.keyence.com/products/measure/laser-1d/cl-3000/; accessed May 24, 2023.